Schweizerische Eidgenossenschaft
Confédération suisse
Confederazione Svizzera
Confederaziun svizra

Eidgenössisches Departement für
Umwelt, Verkehr, Energie und Kommunikation UVEK

Bundesamt für Energie BFE

LAYERED THERMOELECTRIC CONVERTERS

(LTEC)

Jahresbericht 2008

Autor und Koautoren	Laura Bocher and Anke Weidenkaff
beauftragte Institution	Empa
Adresse	Ueberlandstrasse 129
	CH-8600 Duebendorf. Switzerland
Telefon, E-mail, Internetadresse	+41 1 823 41 31, anke.weidenkaff@empa.ch
BFE Projekt-/Vertrag-Nummer	102669 / 153459
BFE-Projektleiter	Anke Weidenkaff
Dauer des Projekts (von – bis)	01.08.2008 – 01.08.2011
Datum	22-11-2008

ZUSAMMENFASSUNG

Thermoelectric oxides are synthesised from liquid precursors which are developed for the purpose of layer by layer thin film deposition technique. As first samples polycrystalline perovskite-type $CaMn_{1-x}Nb_xO_3$ phases (with x = 0.02, 0.05, 0.08 and 0.10) were synthesised and investigated concerning their structure, microstructure and thermal stability as function of the temperature. The studied phases reveal a complex microstructure at room temperature with 90º twinned domains and rock-salt planar defects. At high temperatures, the manganate phases undergo a structural transition from orthorhombic to cubic symmetry as confirmed by in situ high-temperature X-ray powder diffraction and electron diffraction data. Thermogravimetric heating/cooling studies evidence a reversible thermal reduction/re-oxidation process which occurs above a defined transition temperature. From these data, we conclude on a possible mechanism relating the high-temperature structural transition and the thermal reduction process of slightly-substituted $CaMnO_3$ phases. The occurrence of a structural transition can be related to the thermal reduction process, which result in a change of the Mn^{3+}/Mn^{4+} concentrations in the Mn sublattice, and therefore in a modification of the transport properties. A comprehensive study examines for the first time the impact of both phenomena on the electrical and thermal transport properties.

Projektziele

The main objective of the LTEC project is the use of waste heat from combustion processes (exhaust gas, motor, skin) as an energy source. The development of an innovative thermoelectric (TE) system will be based on improved TE materials.

The advantages of an L-TEC compared to thermoelectric converter made by using bulk materials are the improved design-flexibility and better conversion efficiency due to a multi-stage design and graded materials. Thus, L-TEC is an attractive way to convert heat into electrical energy by thermoelectric conversion. This motivation is directly linked to the development of novel functional materials with enhanced Figures of merit, high temperature stability (T ≥ 400 K), and without harmful elements. Here the results from former and running projects will be directly applied for the next generation converters.
A TE module is composed of *p*- and *n*-type thermoelements which are connected electrically in series and thermally in parallel. The efficient conversion of heat into electricity requires the development of functional materials with a high figure of merit, $Z = S^2/\rho\kappa$, where S is the Seebeck coefficient, ρ is the electrical conductivity and κ is the thermal conductivity. Long-term utilizations can be achieved with TE modules since they have the advantage to be maintenance-free. Therefore, the reliability and the durability are essential prerequisites for TE technologies. The chemical, thermal and mechanical stabilities are required with respect to specific operating conditions (temperatures and atmospheres). Oxide thermoelectric materials are cost efficient and nontoxic compared to the conventional phases. They are also chemically and thermally stable at high temperatures in oxidative atmospheres.
Our recent studies on new promising n-type manganate phases, $CaMn_{1-x}Nb_xO_3$ (with x ≤ 0.08), reveal a ZT value of 0.32 at 1070 K as a result of a low lattice thermal conductivity [1]. The study shows that specific internal boundaries and interfaces which are induced by the presence of twinned domains, might decrease the thermal conductivity due to phonon scattering while keeping the electronic properties largely undisturbed. From our knowledge, the electrical and thermal transport properties of both *A*- and *B*-site substituted $CaMnO_3$ have been largely studied only up to T ' 1000 K [2-6]. The higher temperature range (T> 1100 K) has not been explored so far concerning their TE properties. The present paper reports on the study of the , $CaMn_{1-x}Nb_xO_3$ phases (with x = 0.02, 0.05, 0.08 and 0.10), with respect to its crystal structure, microstructure, and thermal stability at high temperatures. Since oxide materials are evaluated regarding their high-temperature thermoelectric applications, the thermal stability of the studied phases is of main interest. The study focuses on the influence of the high-temperature structural transition, the oxygen vacancy formation, and the effects on the electrical and thermal transport properties in the temperature range of 600 K < T < 1250 K.

Durchgeführte Arbeiten und erreichte Ergebnisse

Diverse *n*-type manganate phases were produced with innovative synthesis procedures and thermally cycled. Figures 1a) and b) present the refined high-temperature XRPD patterns of $CaMn_{0.98}Nb_{0.02}O_3$ at 773 K and 1173 K, respectively. The reflections observed at 773 K can be indexed in the orthorhombic unit cell (Pnma S.G., N° 62), while the XRPD data recorded at 1173 K can be refined using the cubic structural model (Pm3m S.G., N° 221).

Figure 2a) depicts the temperature evolution of the $CaMn_{0.98}Nb_{0.02}O_3$ orthorhombic phase. The angular range of 36° < 2 Θ < 43° is emphasized in Figure 2b) since this region includes superlattice reflections

sensitive to the orthorhombic structure and its related tilting system. With increasing temperature, the (201)Pnma, (102)Pnma reflections and the (211)Pnma,(112)Pnma, (131)Pnma triplet decrease in intensity and disappear at 1173 K. The (220)Pnma and (022)Pnma doublet merge to a single (111)Pm-3m reflection at 1173 K. These results indicate that $CaMn_{0.98}Nb_{0.02}O_3$ undergoes a structural transition from orthorhombic to cubic crystal structure at 1073 K < Tc < 1173 K in air. Previous studies on $CaMnO_3$ [7] reported the existence of successive structural transitions from orthorhombic (Pnma) to tetragonal (I4/mcm) at 1169 K and further to cubic (Pm-3m) at 1186 K. In the present case, all orthorhombic superlattice reflections disappear simultaneously at the transition temperature without presence of any intermediate tetragonal phase. The apparent absence of such intermediate transitions for the $CaMn_{0.98}Nb_{0.02}O_3$ phase confirms a limited stability range of the tetragonal phase. Thus, the structural transition temperature determined from the experimental data, i.e. 1073 K < Tc < 1173 K, is consistent with the literature considering the well known transition from orthorhombic to cubic crystal structure upon heating in perovskite-type phases.

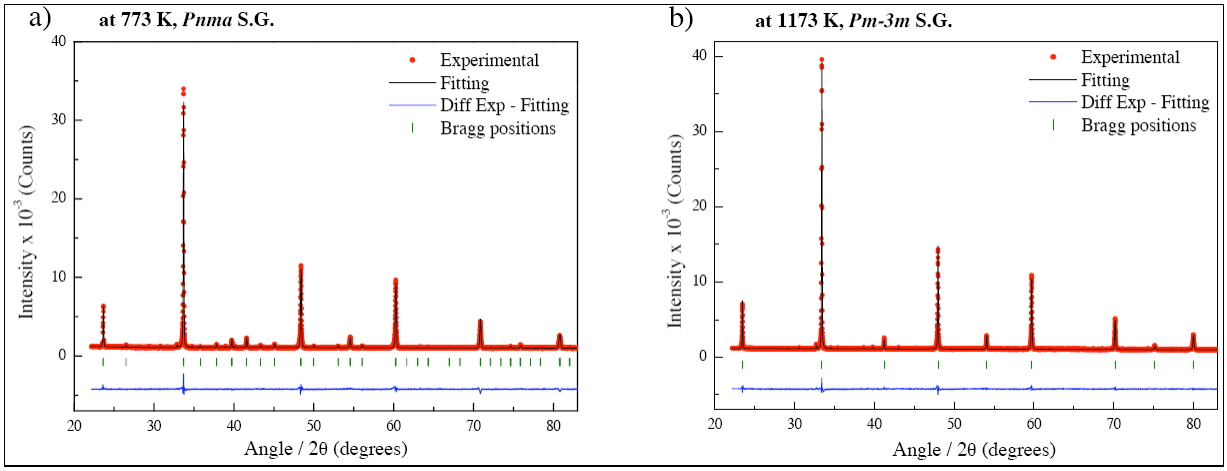

Figure 1: Examples of Rietveld refinements from in situ high-temperature XRPD data of $CaMn_{0.98}Nb_{0.02}O_3$ phase recorded at a) 773 K and b) 1173 K under air atmosphere.

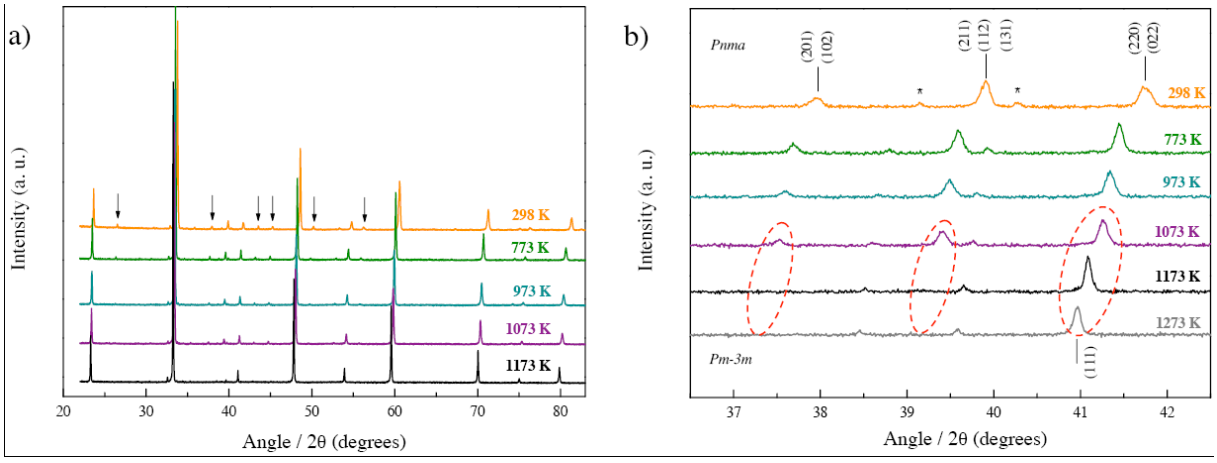

Figure 2: a) and b) In situ high-temperature XRPD patterns of $CaMn_{0.98}Nb_{0.02}O_3$ phase from 298 K to 1173 K under air atmosphere. The arrows in Figure a) indicate the reflections disappearing during the phase transition. The angular range of 36° < 2θ < 43° is enlarged in Figure b) emphasizing the evolution of three main reflections, assigned by red circles, upon heating. The

minor reflections indicated by (*) belong to the secondary phase, i.e. $CaMn_2O_4$. The red dotted circles are only intended to emphasize the reflections of main interest.

The evolution of the lattice parameters and cell volume upon heating are presented in Figure 3a). The thermal expansion causes a near linear increase of lattice parameters for the all studied temperature range. As a consequence, a progressive expansion of the cell volume is observed corresponding to a thermal expansion of 4.40% upon heating from 298 K to 1173 K. Figure 3b) reports on the evolution of average bond lengths (Mn-O) and bond angles (Mn-O-Mn) upon heating. A continuous increase of both structural parameters is observed until the structural transition temperature. This finding reects the thermal expansion of the orthorhombic crystal structure. At higher temperatures, i.e. above Tc, refined bond lengths and angles correspond to values characteristic of the cubic symmetry.

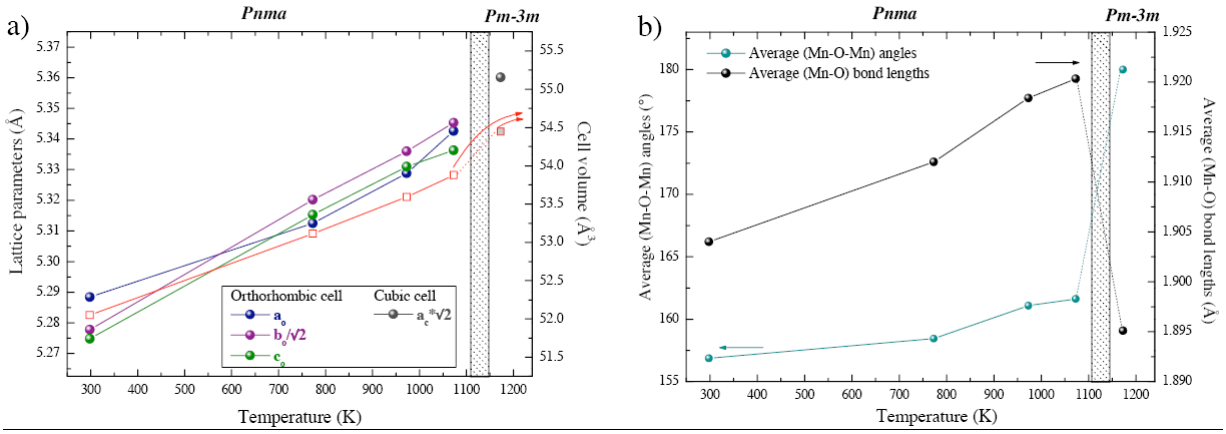

Figure 3: Temperature dependence of a) lattice parameters, cell volumes, b) average (Mn-O-Mn) angles and (Mn-O) bond lengths of the $CaMn_{0.98}Nb_{0.02}O_3$ phase. (The lattice parameters are presented along the orthorhombic frame, where $a_o/\sqrt{2} \sim c_o/\sqrt{2} \sim ac$ and $b_o/2 = ac$. The cell volumes are calculated based on the cubic cell).

With respect to the orthorhombic and cubic crystal structures, it should be pointed out that both symmetries involve divergences from each other regarding the structural parameter, i.e. atomic displacement variations, changes in bond lengths and angles. The ideal cubic perovskite structure, with Pm-3m S.G., rarely exists, often the perovskite structure distorts from the ideal cubic frame arising to orthorhombic or rhombohedral symmetry. The distorted derivative phases result from different mechanisms. One of the most common distortion mechanisms is based on the rotation or tilting of the BO_6 octahedra. Due to the small radius of the A site cation, with respect to its surrounding frame, the BO_6 octahedra tilt and buckle to accommodate the size of the cubo-octahedral void. The co-operative rotation of BO_6 octahedra around different axes yields the orthorhombic, so-called $GdFeO_3$-type structure. In the present case, successive co-operative rotations of the MnO_6 octahedra around the <111> crystallographic axis lead to the orthorhombic crystal structure with Pnma S.G. Consequently, the structural transition induces certainly changes of the overlap between the O 2p and Mn 3d orbitals. Such variation of the electronic band structure leads to modifications of the electrical and thermal transport properties.

The XRPD investigations yield a general overview of the crystal structure and its evolution with increasing temperature. In addition, TEM studies can give a better insight of the local microstructure of the studied materials.

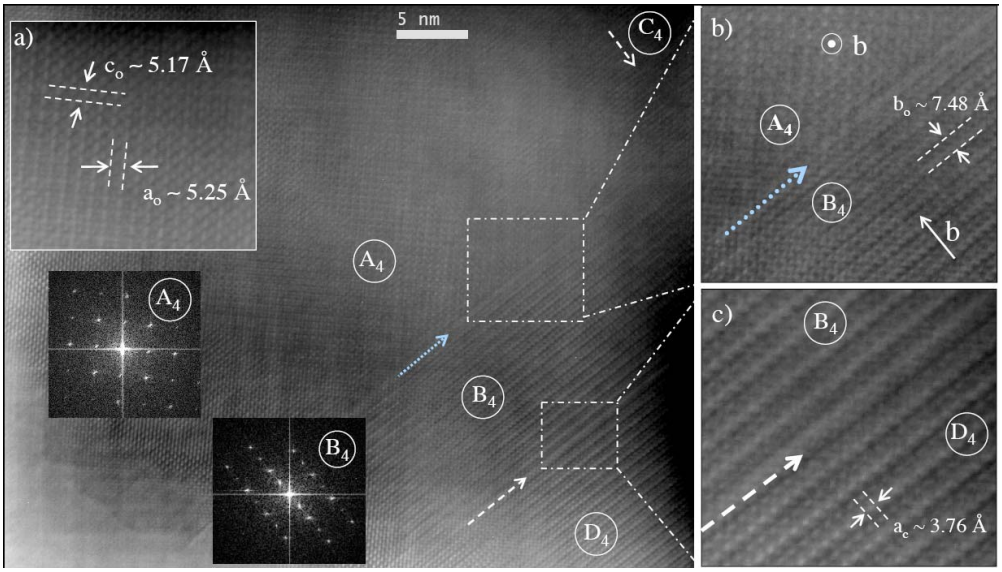

Figure 4: HRTEM images of $CaMn_{0.98}Nb_{0.02}O_3$ phase along a twinned domain boundary, highlight of a) the A_2 domain, b) and c) the boundary separating the domains A_2 and B_2 and the domains B_2 and D_2, respectively. The inset figures present the FFT of the domains A_2 and B_2. Dotted arrows indicate domain boundaries.

An example of specific microstructure observed in the $CaMn_{0.98}Nb_{0.02}O_3$ phase is illustrated in Figure 4a) where the presence of several domain boundaries, assigned as A_2-B_2, B_2-D_2, and A_2-C_2, are indicated by dotted arrows. The A_2-B_2 domain boundary is highlighted in Figure 4b) and their FFTs are given in the inset Figure 4a). They allow to confirm the presence of twinned domains where the b-axis is either oriented out of the plane (A_2) or in the plane (B_2). The *b*-axis rotates by 90° across $[101]_o$ (Cf Schlussbericht 2008). Between the B_2-D_2 regions, characteristic features of twinned domains are not observed, as presented in Figure 4c). In both domains, the b-axis is oriented in the same direction and the lattice fringes present similar values (b ~ 0.74 nm).Contrast differences which should emerge between twinned domains, are not observed between both regions. However, the B_2-D_2 defect boundary appears clearly with unusual interdistance equivalent to twice the b-axis length. This domain boundary between the B_2-D_2 regions might be due to an intergrowth Ruddlesden-Popper planar defect involving anti-phase boundaries [8]. Ruddlesden-Popper series are well-known as layered perovskite-type structure $A_{n+1}B_nO_{3n+1}$ with n the number of AO layers. Thus, perovskite-type manganate phases such as $CaO[(CaM_nO3)_n]$ could be a planar defect structure localized between the B_2-D_2 regions.

In addition to the high-temperature XRPD measurements, in situ high-temperature ED of the $CaMn_{0.98}Nb_{0.02}O_3$ phase was performed focus on a zone axis which comprises information about the long b-axis, characteristic of the orthorhombic structure with Pnma S.G. In Figure 5a), the experimental ED pattern, recorded at room temperature, is indexed in the orthorhombic phase with the [10-1]o zone axis. The additional set of diffraction spots, indicated with red rings, confirms the b-axis orienta-

tion. The high-temperature ED pattern, shown in Figure 5b), can be indexed in the cubic perovskite structure, i.e. with $[001]_c$ zone axis, since any additional set of diffraction spots is observed. The diffraction patterns were carefully recorded on the same region of the particle at room temperature and at T = 770 K. This result confirms the evidence of a structural transformation from orthorhombic to cubic structure with increasing temperature, as concluded from the structural Rietveld refinements. Since the [010] 90° rotation twins are a characteristic microstructure of the orthorhombic structure, dewinning phenomenon occurs by reduction of the fourfold rotation axis during the structural transition upon heating [9].

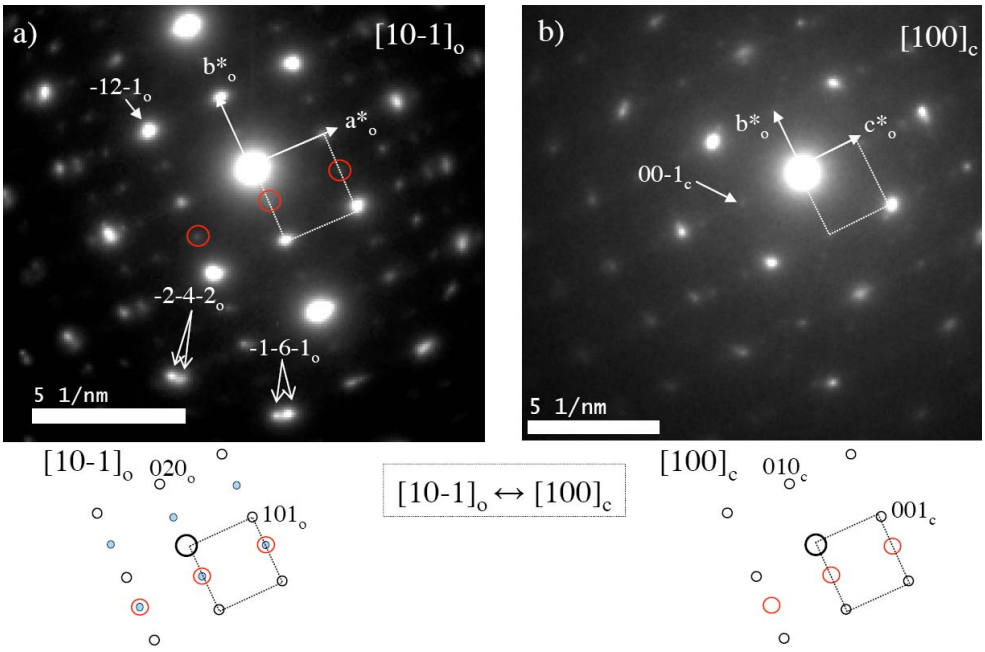

Figure 5: In situ high-temperature ED of $CaMn_{0.98}Nb_{0.02}O_3$ phase recorded a) at 298 K and b) 770 K. Schematic interpretations of the ED patterns are represented below the figures.

The potential thermoelectric manganate phases, i.e. $CaMn_{1-x}Nb_xO_3$ ($x < 0.10$), were investigated by thermogravimetric analyses regarding their thermal stability at high temperatures. Successive in situ thermal cycles were performed on the $CaMn_{0.98}Nb_{0.02}O_3$ phase under synthetic air atmosphere until T = 1253 K. Figure 6a) reveals a weight loss upon heating and a gain of weight upon cooling recovering the starting sample weight. The loss/gain of weights are related to a reversible oxygen release/uptake, respectively. The subsequent and reproducible thermal reduction and re-oxidation processes occur above T_{HT} = 1090 K. (Hereafter, the onset temperature relating to the thermal reduction will be termed T_{HT}). From the thermogravimetric data, the oxygen deficiency δ is determined to be equal to $0.045 < \delta < 0.049$ up to 1253 K. No further oxygen release is observed while sustaining the compound at T > THT for a one-hour isothermal step. Similar investigations on the $CaMn_{1-x}Nb_xO_3$ phases present a shift of THT to higher temperatures with increasing the Nb content, i.e. for x = 0.05: THT~1145 K and for x = 0.08: THT ~ 1180 K, as reported in Figure 6b).

Hence, the thermal stability of the $CaMn_{1-x}Nb_xO_3$ phases can be fine-tuned depending on the Nb substitution levels. Furthermore, the onset of the thermal reduction temperature THT apparently corresponds to the structural transition temperature T_c. A possible mechanism relating the structural transition and the thermal reduction is proposed. On one hand, detwinning phenomena cause structural

reconstructions where domain boundaries disappear to accommodate the cubic structure. On the other hand, small amount of oxygen might be released at the twinned domain boundaries. Hence, the oxygen vacancy formation and the detwinning of the orthorhombic structure might be interdependent phenomena.

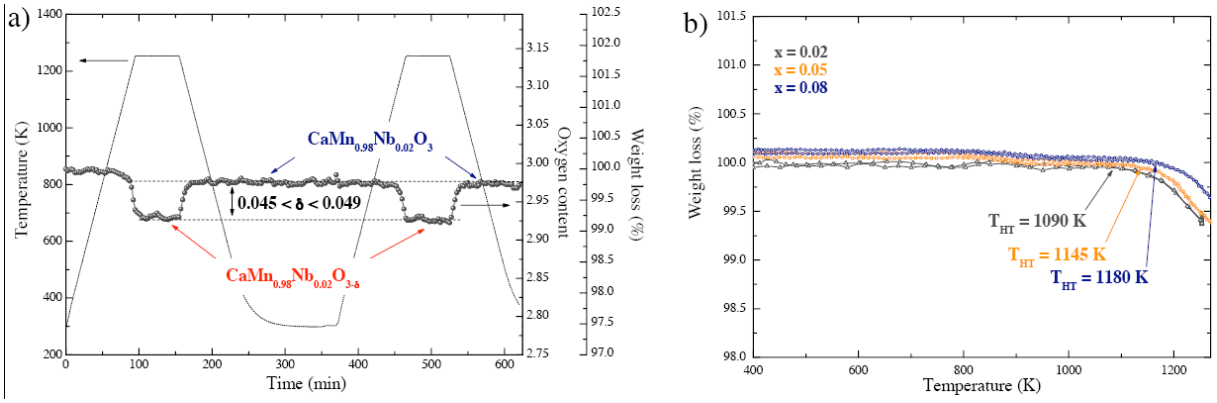

Figure 6: In situ thermogravimetric analyses of a) CaMn0.98Nb0.02O3 and b) CaMn1-xNbxO3 (with x = 0.02, 0.05, and 0.08) phases upon heating and cooling cycles under synthetic air atmosphere. Two successive thermal cycles including an one-hour isothermal step at T = 1253 K are presented in Figure a).

Figure 8 presents the temperature dependence of the Seebeck coefficient for the $CaMn_{1-x}Nb_xO_3$ series (for x = 0.02, 0.05, 0.08 and 0.10). Equal thermopower values are obtained upon heating and cooling processes under ambient air atmosphere. This finding indicates that no gradual deterioration of the compounds and their related TE properties occur after several thermal cycles up to 1273 K. Two different *S*(T) behaviors can be distinguished in the studied temperature range for all compositions. The low-temperature region presents a nearly linearly temperature dependent thermopower, characteristic of a polaronic conduction [1]. A drop of the absolute Seebeck coefficient values is observed above a certain boundary temperature, as indicated by the dotted line on the Figure. The comparison of the thermopower curves for all the studied compositions suggests that an increase of the Nb concentration yields a shift of the S(T) drop to higher temperatures, e.g. from T_{HT} = 1090 K for x = 0.02 to T_{HT} = 1200 K for x = 0.10. In analogy to the thermogravimetric results, this boundary temperature can be assigned to the onset temperature of the thermal reduction process T_{HT}. The sudden change of *S*(T) slope at T ~ T_{HT} indicates a modification of the electronic conduction in the high-temperature region.

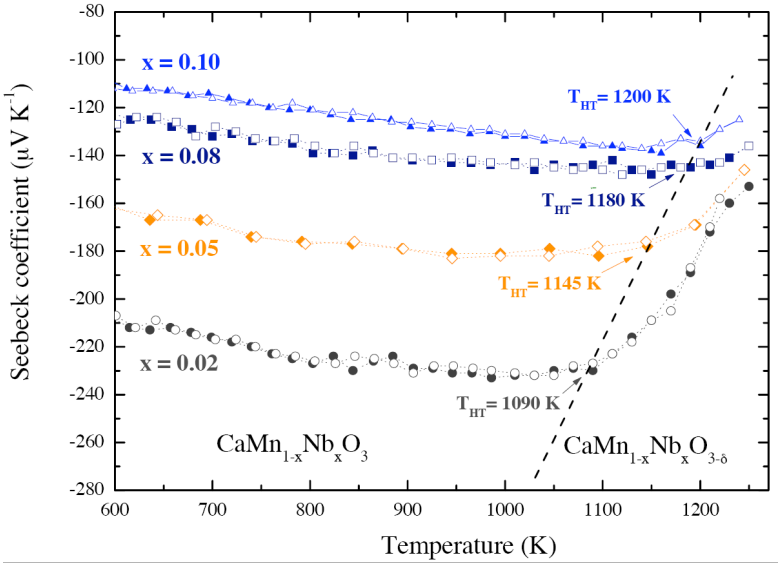

Figure 7: Temperature dependence of Seebeck coefficient for $CaMn_{1-x}Nb_xO_3$ (for x = 0.02, 0.05, 0.08 and 0.10) while heating (closed symbols) and cooling (open symbols) under air atmosphere. The dotted line is just intended to guide the eye regarding the transition temperature evolution.

The decrease of the thermopower, above the transition temperature, can be interpreted either as a modification of the band structure due to the structural transition or as an increase of the Mn^{3+} concentration in the Mn^{4+} matrix related to the thermal reduction. the thermal reduction induces oxygen-deficient compounds in which the concentration of Mn^{3+}/Mn^{4+} varies to satisfy the electroneutrality. As a result, upon cooling, the thermal re-oxidation allows to recover the starting Mn^{3+} concentration at room temperature, inducing identical S(T) values after several thermal cycles.

Figure 8a) presents the temperature dependence of the electrical resistivity for the $CaMn_{1-x}Nb_xO_3$ phases with x = 0.02, 0.05, and 0.08. The ρ(T) curve of the 2% Nb-containing $CaMnO_3$ first presents a slope change at T ~ 800 K leading to nearly constant resistivity values. This could be considered as the onset of the structural transition. At T > 1050 K, a decrease of ρ (T) is clearly observed and its to the thermopower drop observed at this temperature, as indicated by the dotted line on the Figure. This last finding confirms the variation of charge carriers concentration in terms of an increase of the Mn^{3+} concentration above T_{HT}. Similar change of ρ (T) slopes is observed for the 5% Nb- and 8% Nb-containing $CaMnO_3$ phases. A shift of the resistivity drop to higher temperatures is observed with increasing the Nb concentrations as a common feature with the thermopower data, and further with the onset temperature of the thermal reduction. Hence, the high-temperature TE properties of the $CaMn_{1-x}Nb_xO_3$ phases are clearly dependent on their thermal stability.

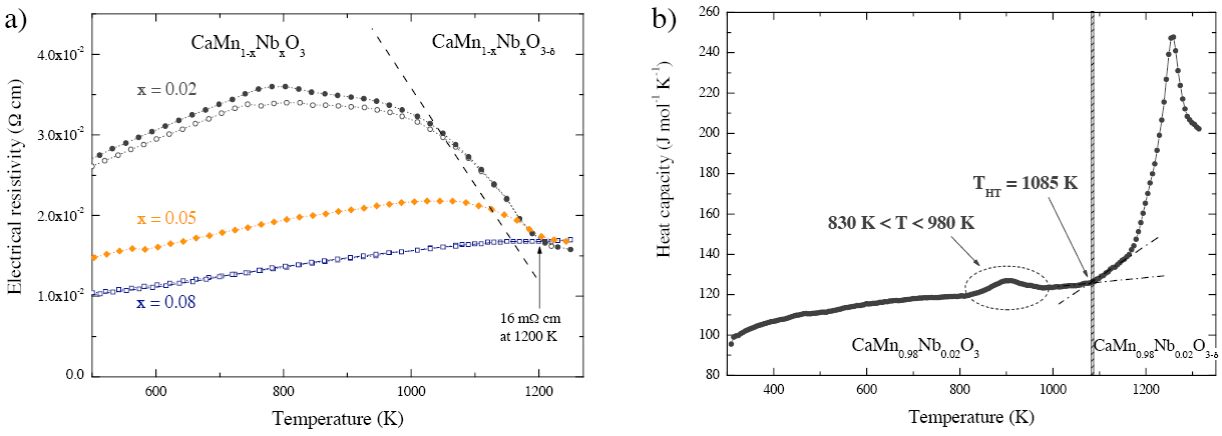

Figure 8: a) Temperature dependence of electrical resistivity for $CaMn_{1-x}Nb_xO_3$ (for x = 0.02, 0.05 and 0.08) while heating (closed symbols) and cooling (open symbols) under air atmosphere and b) Specific heat capacity temperature dependence of $CaMn_{0.98}Nb_{0.02}O_3$. The dotted line is just intended to guide the eye regarding the transition temperature evolution.

The heat capacity study performed on the 2% Nb-containing $CaMnO_3$ phase is reported in Figure 9b). The manganate phase undergoes two successive endothermic thermal events, at 830 K < T_1 < 980 K and at T_2 > 1085 K, upon heating to 1273 K in ambient air atmosphere. The second peak is energetically more significant than the first one. DSC methods allow to monitor enthalpy variations and therefore to observe structural transitions [10]. However, DSC measurements are also sensitive to thermal reduction events since this process induces changes of the anionic composition. In analogy with the

resistivity data, the first peak (T_1) can be assigned to the onset temperature of the structural transition and the second one (T_2) corresponds to the onset temperature of the thermal reduction process. Since different heating rates were used depending on the characterization methods, these assumptions should be carefully considered.

Nationale Zusammenarbeit

- Prof. K. Fröhlich, High Voltage Technology Laboratory, ETHZ. Theoretical descriptions correlated with experiments and modelling with A. Bitschi.
- Dr. L. Castaldi and Prof. Ch. Baerlocher, Laboratory of Crystallography ETHZ. High temperature X-ray powder diffraction measurements on manganate-type perovskite structure (up to 1200°C)

Internationale Zusammenarbeit

- Dr. A. Maignan, Dr. S. Hébert, CRISMAT laboratory, UMR 6508 CNRS/ENSICAEN - France. Thermoelectric properties on complex oxide structures at high and low temperatures.
- Dr. J. Hejtmanek, Institute of Physics ASCR, Prague - Czech Republic. Thermal properties on oxide materials.
- Dr. S. Bakardjieva, Institute of Inorganic Chemistry of the ASCR, Czech Republic. High temperature transmission electron microscopy.

Bewertung 2008

The present study reveals that the $CaMn_{1-x}Nb_xO_3$ ($x < 0.10$) phases undergo a thermal reduction and a structural transition from orthorhombic to cubic symmetry at high temperatures, both phenomena being reversible upon cooling. Increasing the Nb content in the $CaMnO_3$ structure results in a shift of the thermal reduction onset temperature to higher temperatures. Thus, the $CaMn_{1-x}Nb_xO_3$ phases are thermally stable up to a high-temperature limit, i.e. T_{HT} = 1090 K for x = 0.02 to T_{HT} = 1200 K for x = 0.10. The microstructure of the $CaMn_{0.98}Nb_{0.02}O_3$ phase is characterized at room temperature by different features, i.e. the presence of twinned domains and rock-salt planar defects. (i) Twinned domains present in the orthorhombic crystal structure corresponds to 90° rotation twins across f101go. The rotation twins are often observed in orthorhombic phases which undergo structural transition from higher to lower symmetry upon cooling. The structural transition induces a detwinning of the crystal structure at high temperatures which might be related to small oxygen release at the domain boundaries. (ii) The microstructure of the $CaMn_{0.98}Nb_{0.02}O_3$ phase reveals also intergrowth Ruddlesden-Popper planar defects involving anti-phase boundaries.

Furthermore, electrical and transport properties of the $CaMn_{1-x}Nb_xO_3$ ($x < 0.10$) phases present serious changes at high temperatures. Lower absolute Seebeck coefficient and electrical resistivity values are observed in the high-temperature range, indicating an enhancement of the electrical conduction. For instance, the thermopower evolution in the high-temperature region can be well explained based on the oxygen vacancy formation. Moreover, the changes in S(T) and ρ(T) are observed at higher temperatures with increasing the Nb concentration since the thermal stability of the $CaMn_{1-x}Nb_xO_3$ phases increases with the Nb extent. Hence, the thermoelectric properties of the manganate phases

can be further fine-tuned regarding their temperature of applications. In addition, the manganate phases does not reveal any degradation of their thermoelectric properties even after several heating/cooling cycles up to 1273 K since they reveal complete and reversible oxygen release/uptake capabilities.

Referenzen

[1]. L. Bocher, M. H. Aguirre, D. Logvinovich, A. Shkabko, R. Robert, M. Trottmann, and A. Weidenkaff, Inorg. Chem., 2008, 47, 8077-8085.

[2]. T. Kobayashi, H. Takizawa, T. Endo, T. Sato, and M. Shimada J. Solid State Chem., 1991, 92, 116-129.

[3]. M. Ohtaki, H. Koga, T. Tokunaga, K. Eguchi, and H. Arai, J. Solid State Chem. 1995, 120, 105-111.

[4]. L. Pi, C. Martin, A. Maignan, and B. Raveau, Phys. Rev. B 2003, 67, 02443 1-7.

[5]. P. X. Thao, T. Tsuji, M. Hashida, and Y. Yamamura, J. Ceram. Soc. Jap. 2003, 111, 544-547.

[6]. D. Flahaut, T. Mihara, R. Funahashi, N. Nabeshima, K. Lee, H. Ohta, and K. Koumoto, J. Appl. Phys., 2006, 100, 084911 1-4.

[7]. H. Taguchi, M. Nagao, T. Sato, and M. Shimada, J. Solid State Chem. 1989, 78, 312-315.

[8]. G. C. Mather, F. M. Figueiredo, J. Romero de Paz, and S. Carcia-Martin Inorg. Chem. 2008, 47, 921-929.

[9]. W. L. Wang, and H. Y. Lu, J. Am. Ceram. Soc. 2006, 89, 281-291.

[10]. M. H. Aguirre, D. Logvinovich, L. Bocher, R. Robert, S. G. Ebbinghaus, and A. Weidenkaff, Acta Mater., 2008.

List of conference contributions and scientific publications in the 2008 funding period:

Publications

1. "$CaMn_{1-x}Nb_xO_3$ ($x \leq 0.08$) Perovskite-Type Phases As Promising New High-Temperature *n*-Type Thermoelectric Materials." L. Bocher, M. H. Aguirre, D. Logvinovich, A. Shkabko, R. Robert, M. Trottmann, and A. Weidenkaff. *Inorg. Chem.,* **2008**, 47, 8077-8085.

2. "High-temperature thermoelectric properties of Sr_2RuYO_6 and Sr_2RuErO_6 double perovskites influenced by structure and microstructure." M. H. Aguirre, D. Logvinovich, L. Bocher, R. Robert, S. Ebbinghaus, and A. Weidenkaff. *Acta Materialia*, **2008**, doi:10.1016/j.actamat.2008.09.003

3. "Structure, microstructure and high temperature transport properties of $La_{1-x}Ca_xMnO_3$ thin films and polycrystalline bulk materials". M H. Aguirre, S. Canulescu, R. Robert, N. Homozava, D. Logvinovich, L. Bocher, Th. Lippert, M. Döbeli and A. Weidenkaff. *J. Appl. Phys.* 103, **2008**, 013703 1-6.

4. “Thermoelectric and magnetic properties of perovskite-type manganate phases synthesised by ultrasonic spray combustion (USC)”. L. Bocher, R. Robert, M. H. Aguirre, S. Malo, S. Hébert, A. Maignan and A. Weidenkaff. *Solid State Sciences*, 10, **2008**, 496-501.

5. “Thermoelectric properties of $LaCo_{1-x}Ni_xO_3$ polycrystalline samples and epitaxial thin films”. R. Robert, M. H. Aguirre, L. Bocher, M. Trottmann, S. Heiroth, Th. Lippert, M. Döbeli and A. Weidenkaff. Solid State Sciences. *Solid State Sciences*, 10, **2008**, 501-507.